Engineering Science and Technology, an International Journal 43 (2023) 101435

HOSTED BY

Contents lists available at ScienceDirect

Engineering Science and Technology, an International Journal

journal homepage: www.elsevier.com/locate/jestch

Experimental analysis of phase shift modulation methods effects on EMI in dual active bridge DC-DC converter

Samet Yalçın [a,*], Tuna Göksu [a], Selami Kesler [a,b], Okan Bingöl [a]

[a] Department of Electrical and Electronics Engineering, Isparta University of Applied Sciences, Turkey
[b] Department of Electrical and Electronics Engineering, Pamukkale University, Turkey

ARTICLE INFO

Article history:
Received 1 March 2022
Revised 3 April 2023
Accepted 3 May 2023
Available online 19 May 2023

Keywords:
Dual active bridge (DAB) converter
Phase shift modulation (PSM)
Electromagnetic interference (EMI)
Conducted EMI
Wide bandgap (WBG)
Semiconductors

ABSTRACT

Dual active bridge DC-DC converters (DAB) are one of the bidirectional converters and mainly used in electric vehicles and micro grids. With the increasing number of electric vehicles in use, and the increasing amount of batteries in these vehicles and rapidly spanning micro grids, the importance of DAB converters has increased and they are expected to be smaller in size and operate at higher power levels. The reduction in size has increased the importance of power density and efficiency, which are two significant parameters of DAB circuits. One of the methods to increase efficiency and power density is to increase the switching frequency. However, with the increase at the switching frequency, electromagnetic interference (EMI) in the DAB circuit also increases.

In this manuscript, the change in the EMI values emitted by conduction, according to the phase shift modulation methods at DAB converters are evaluated. Also the effect of type of MOSFETs on conducted EMI is examined. Prototypes of the DAB converters by using Si and SiC MOSFETs with power rating of 1 kW are designed and developed. Switching frequency of converter is 25 kHz and leakage inductance is determined 81uH and 75uH. Si based circuit is operated with %88.5 efficiency. SiC based circuit is also operated with %88 efficiency. The designed circuits are operated using the phase shift modulations SPS and DPS. Conducted emission noise emitted by these circuits are analyzed by dividing them into common mode and difference mode noises. It has been observed that the EMI value when using SPS method is 15–20 dBμV lower than the EMI when using DPS method. The relationship between the measured noises and the efficiency of the circuits was observed.

1. Introduction

Due to the rising energy demand and the necessity of using energy efficiently, the importance of efficiency and power density in power electronics in areas such as space, aviation, electric vehicles and energy storage is increasing day by day. In order to increase the power density, it is necessary to perform switching at high frequencies. However, since switching at high frequencies will increase the dv/dt and di/dt ratios, it creates transient voltage and current noises in parasitic inductances and capacitances [33]. The device operating at high frequencies may damage other systems or equipment with which it works due to the electromagnetic interference (EMI) it creates.

EMI can be emitted by radiation or by conduction [5,1,8]. In power electronics circuits, conducted emission is examined in two separate parts as common mode (CM) and differential mode (DM). The source of CM noises is the parasitic components between the circuit lines and the ground while non-zero ESR of capacitances causes DM noises. There are many studies in the literature showing that CM noise is much higher than DM noise. Therefore, CM noise has a greater effect than DM noise when examining EMI [23,6].

When the literature is examined in terms of efficiency, it is seen that double active bridge (DAB) DC-DC converters have an important place in DC-DC converters used at high power [30,19,7,10]. However, DAB circuits are complex since they have 8-switching control structure, and also their EMI values are high due to their output capacitance values [13]. DAB circuits are controlled by four different phase shift modulation methods: single phase shift (SPS), dual phase shift (DPS), extended phase shift (EPS) and triple phase shift (TPS) modulation. Although it is seen that SPS is widely used in the literature [11], especially the TPS modulation method maintains its importance in terms of efficiency and in-depth control. In addition, there are studies in the literature showing that the EMI values of the DAB circuits used with the SPS switching method are higher than the circuits with different topologies [13].

* Corresponding author.

https://doi.org/10.1016/j.jestch.2023.101435
2215-0986/

There are six articles that analyzed EMI on DAB converters. In the first paper, Si based neutral point clamped (NPC) DAB was analyzed by Kumar [20]. EMI was attenuated by using dv/dt parameters. But phase shift method was not mentioned. In the other study, Dwiza simulated a DAB converter on LTspice and she reduced the EMI by using symmetrical leakage inductance only on simulation program [6]. However Chu [3] had already showed some leakage inductance techniques for reducing EMI.

Geramirad [9] explained EMI results of a 1200 V SiC based DAB converter. Besides he mentioned the EMI reduction by control of gate driver. But he didn't analyze the effect of phase shift modulations on EMI. Heller [12] studied on EMI filter for three-phase DAB converter. Also Kumar renewed his common-mode current cancelation technique study in 2019 and he presented an article in 2022 [21]. In the paper, he showed the Active Neutral Point Clamped (ANPC)-based parallel DAB system with a single phase DAB circuit with an example of SPS, EPS, DPS and TPS modulation methods. Then he has chosen TPS method because this method may help in reducing CM current peaks by switching at lower current. So he used ANPC-based parallel DAB circuit with TPS modulation method in this study. He applied hardware CM suppression methods such as snubber capacitor and CM choke, which have examples in the literature and also reduce the efficiency by reducing the dv/dt ratio, and published the results. Therefore, in this paper, the effect of hardware studies on EMI is studied, and the effect of software and modulation studies on EMI is not given. And then an equivalent circuit model is established to predict the EMI [36]. But a research is not done to reduce EMI in this study.

When we read this state-of-art papers we can notice that no one analyzed the effect of phase shift modulation techniques on EMI however, these techniques are quite important. Because if you need to reduce EMI, you could suppress using analyzed phase shift modulation methods without making a hardware process such as gate drive control and EMI filter design. In this paper, the effects of SPS and DPS methods on EMI are analyzed on the same DAB circuit.

In this study, two DAB circuits using Si and SiC MOSFETs with power rating of 1 kW and 80 V output voltages are designed. These designed circuits controlled by SPS and DPS modulation techniques separately were analyzed at LTspice program, and then EMI analyzes of the circuits were carried out experimentally. In section II, four DAB circuits designed with Si and SiC MOSFETs controlled with SPS and DPS modulation methods are explained. In section III, the operating parameters of DAB circuits which are leakage inductance current, input power, power loss and efficiency are compared with each other. In section IV, EMI of the designed circuits are analyzed. In section V, the EMI of the DAB circuits in 150 kHz-108 MHz spectrum range has been investigated experimentally. In section VI, the results of this study is explained.

2. Modelling and design of DAB circuit

In DAB circuit the power transfer across leakage inductance is the same as the power transfer across an inductance between two voltage source with a phase difference between each other. So the direction and magnitude of the power is transferred are controlled by the phase difference between the voltage source as shown in Equation (1) [30,11].

$$P_o = \frac{V_{HV} V_{LV} \sin\varphi}{\omega L} \tag{1}$$

here P_o is the transmitted power or output power, V_{HV} is the voltage of the DC voltage source located in the high voltage part of the DAB converter, V_{LV} is the voltage of the DC voltage source located in the low voltage part of the DAB converter, φ is phase difference between V_1 and V_2, ω is the radial switching frequency, and L is defined as the total leakage inductance (the sum of the transformer leakage inductance and the inductance connected in series with the transformer).

Similarly, power transfer in DAB circuit is accomplished by generating square waves on the high voltage and low voltage sides by MOSFET's. If the phase between square waves is shifted, the transferred power can be controlled like phase difference. According to this, Equation (5), 6 and 7 is generated from Equation (1).

In this paper, the DAB circuits designed are controlled with SPS and DPS modulation techniques. In the circuits designed, IRFP460s are used as Si MOSFETs. For SiC MOSFET DAB circuits, Wolfspeed C2M0160120D MOSFETs are used in high voltage side and Wolfspeed C2M0080120D MOSFETs are used in low voltage side [32]. In addition, with the modulation techniques applied, the leakage inductance current of the circuit shown in Fig. 1 can be changed.

The phase shift range is not indicated by the φ phase shift angle in this study. Instead it is indicated by the phase shift ratio $D = \varphi/\pi$, which is used in many studies. The phase shift ratios of the modulation techniques used in the DAB circuits are called D_1, D_2 and D_3. D_1 is the internal phase shift ratio of the H bridge on the left side of the transformer, according to the circuit given in Fig. 1. D_2 is the internal phase shift ratio of the H-bridge on the right side of the transformer, again according to Fig. 1. D_3 is the external phase shift ratio between the H bridges.

Voltage conversion ratio (d) should be checked for soft switching. The voltage conversion ratio is defined the voltage ratio on

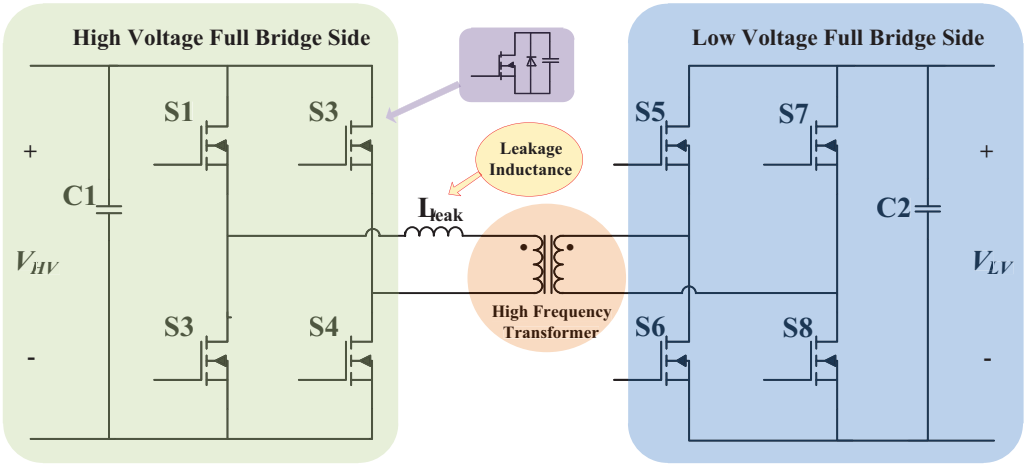

Fig. 1. DAB DC-DC Converter.

both sides of the leakage inductance as given Equation (2). Even though the conditions for soft switching of the voltage conversion ratio and the phase shift ratio (D_3) have been specified in the literature, it has been accepted in many papers that if the voltage conversion ratio is equal to one, DAB converter is operated in soft switching regardless of phase shift ratio [30,13,34,17].

$$d = \frac{V_{HV}}{N_{ps} \times V_{LV}} \tag{2}$$

here d is voltage conversion ratio, V_{HV} is the voltage of high voltage side and V_{LV} is the voltage of low voltage side of leakage inductance as shown in Fig. 1. N_{ps} is winding ratio of the transformer. The condition for zero voltage switching (ZVS) soft switch are obtained in terms of phase shift ratio (D_3) and voltage conversion ratio of DAB converter as shown in Equation (3) and Equation (4) for high voltage bridge side and low voltage bridge respectively [30,34]

$$D_3 > \frac{1}{2}(1-d) \tag{3}$$

$$D_3 > \frac{1}{2}(1-\frac{1}{d}) \tag{4}$$

In this study, V_{HV} is 200 V, V_{LV} is 80 V, D_3 is 0.15 and N_{ps} is 2 in order to accomplish soft switching for both of bridges. However, it should be noted that the loss may not be at the minimum when the circuit operates with soft switching [24].

2.1. SPS modulation method in DAB circuit

This method is referred to as the traditional method in the literature [11]. In this method, while phase shifting is performed between H bridges (between S1 and Q1 switches) ($D_3 \neq 0$), there is no phase difference between the half bridges ($D_1 = D_2 = 0$). In this method, a difference of half of the period ($T_{hs} = \frac{T_s}{2}$) is always created between S1-S3, S2-S4, Q1-Q3 and Q2-Q4 MOSFETs. For the outer phase shift ratio, a gap of ($D_3 T_{hs}$) is created between S1 and Q1 [18,27,2].

The relationship between the power transferred in SPS modulation and the external phase shift ratio D_3 is given in Equation (5) [2,35].

$$P_o = \frac{nV_{HV}V_{LV}}{2f_{sw}L} D_3(1-D_3) \tag{5}$$

here P_o, V_1, V_2 and L are defined in explanation of Equation (1). n is the transformer winding ratio (Np/Ns), D_3 is the external phase shift ratio between the two full bridges and f_{sw} is the switching frequency.

It is known that common mode noise is generated at the rise time of switching [30,14]. Therefore, switching frequencies of Si and SiC based DAB converter should not be different for correct EMI comparison between circuits. Moreover, according to Table 1, SiC MOSFET's can operate above 100 kHz efficiently but Si MOSFET's cannot operate above 40 kHz efficiently. For that reason, the switching frequency is selected 25 kHz for both Si based and SiC based DAB converter circuits.

Table 1
Efficiency Comparison of Si and SiC Isolation Converters and Inverters [29,15].

Material	Switching Frequency (kHz)	Efficiency (%)	Topology
Si	40	98	VSI
	100	96	VSI
SiC	40	99	VSI
	100	99	VSI
	200	97.5	DAB
	250	97.3	DAB

In this study, for a DAB circuit which has 200 V input voltage, 80 V output voltage, 1 kW nominal output power, transformer with winding ratio of 2 and 25 kHz switching frequency, D_3 phase shift ratio is calculated as 0.15 and total leakage inductance is calculated as 81μH.

The PCB design of the DAB circuit was made in the KiCad program as shown in Fig. 2. Afterwards, the circuit was produced as shown in Fig. 3. The designed circuits are controlled by STM32F407 microprocessor.

2.2. DPS modulation method in DAB circuit

This technique was first proposed by [2]. Main difference of this modulation method from SPS is that the phase shift ratios within the H bridges are not zero ($D_1 = D_2 \neq 0$). However, it should be

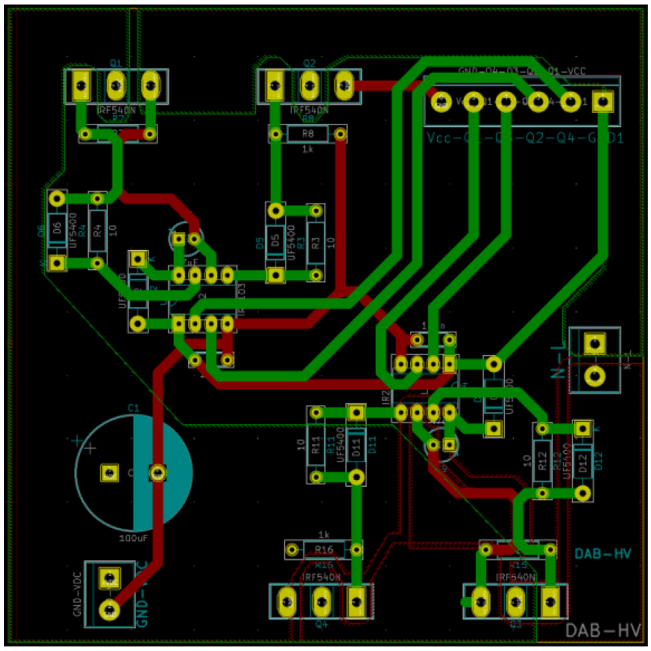

(a)

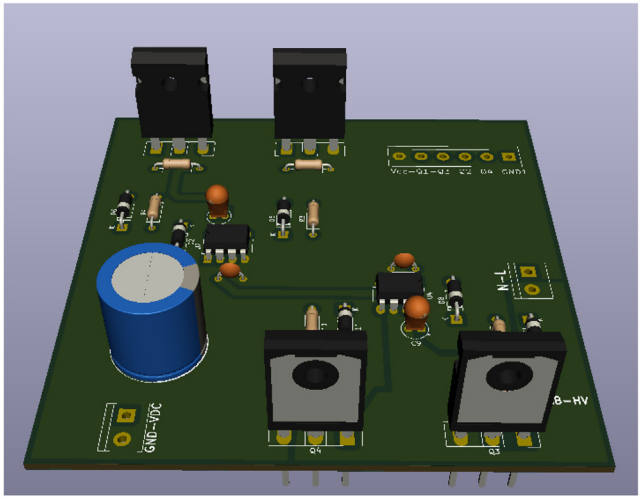

(b)

Fig. 2. DAB Devresi (a) PCB of High Voltage Circuit, (b) 3D Image of DAB Circuit.

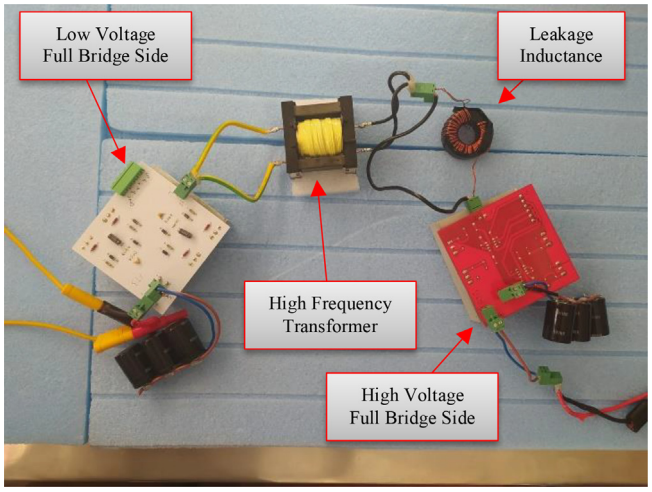

Fig. 3. The Design of DAB DC-DC Converter.

noted that in this method, the phase shift ratios of both H bridges should be equal to each other.

The desired output power formula in the DPS modulation method is explained in two conditions according to the relationship between the phase shift ratio between bridges (D_3) and the phase shift ratios within the bridges (D_1, D_2) as given in Equation (6) and Equation (7) [35,11].

$$P_o = \frac{nV_{HV}V_{LV}}{2f_{sw}L}\left(D_3(1-D_3) - \frac{1}{2}{D_1}^2\right),\ 0 \le D_1 \le D_3 \le 1 \tag{6}$$

$$P_o = \frac{nV_{HV}V_{LV}}{2f_{sw}L}D_3\left(1 - D_1 - \frac{1}{2}D_3\right),\ 0 \le D_3 \le D_1 \le 1 \tag{7}$$

In this formula D_1 is the phase shift ratio in high voltage H bridge circuit and D_2 is the phase shift ratio in low voltage H bridge circuit. In order to obtain a design with the same external phase shift ratio (D_3 = 0.15) at the same input and output values, Equation (6) is calculated as $D_1 = D_2 = 0.1$ and leakage inductance as 75uH. The circuit diagram and PCB printing were carried out as the same as the previous circuit.

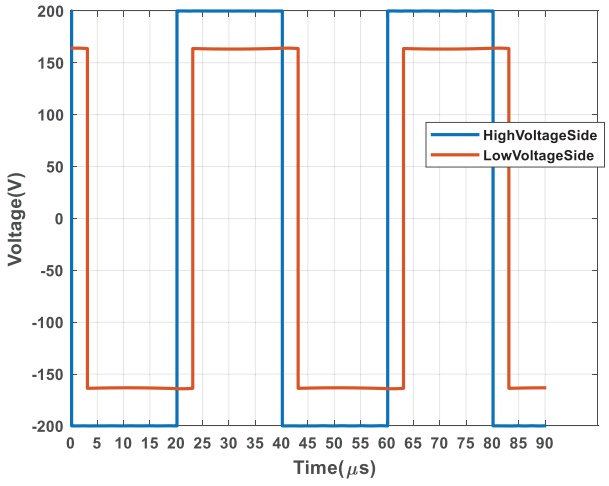

(a)

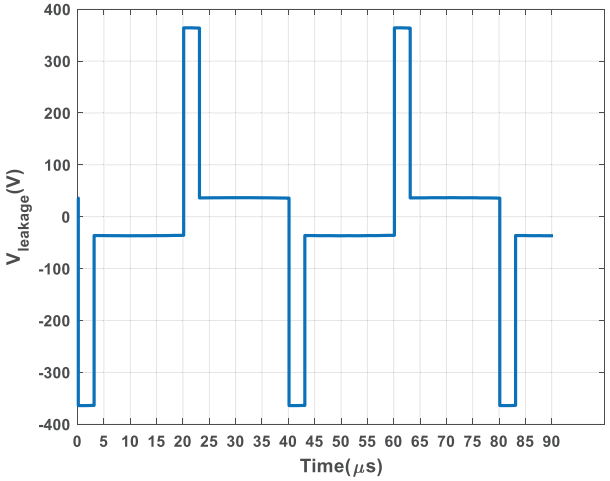

(b)

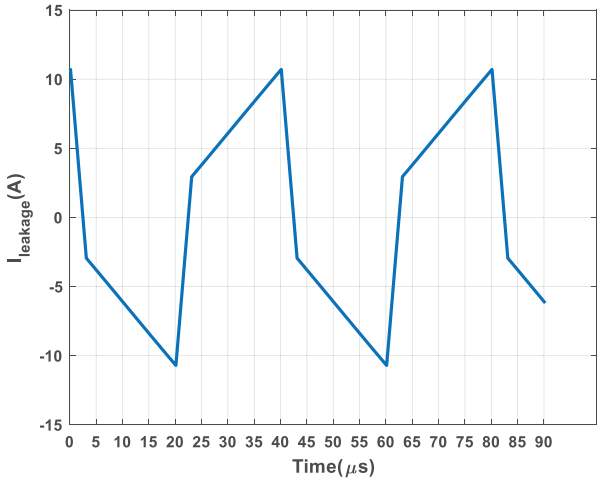

(c)

Fig. 4. Current on Leakage Inductance of Si Based DAB Circuit Operating with SPS Modulation Method.

3. Experimental results

The H bridge MOSFETs of DAB circuit are symmetrical with each other, so the relationship between the leakage inductance current and the high circuit MOSFETs current is as shown in Equation (8) [16,15].

$$I_{DAB(RMS)} = \sqrt{I^2_{M1(RMS)} + I^2_{M2(RMS)}} \tag{8}$$

$I_{DAB(RMS)}$ is the leakage inductance RMS current, $I_{M(RMS)}$ is the MOSFET's RMS current. If the MOSFETs are identical, their current formula is given as shown in Equation (9) [16].

$$I_{M(RMS)} = \frac{I_{DAB(RMS)}}{\sqrt{2}} \tag{9}$$

Therefore, if the R_{DSon} resistances of the switching elements are known in the circuit, the conduction loss can be calculated with Equation (10) [23].

$$P_{Cond\_loss\_total} = 4 \times {I_{DSon\_RMS}}^2 \times R_{DSon} + 4 \times (N \times I_{DSon\_RMS})^2 \times R_{DSon} \tag{10}$$

here $P_{Cond\_loss\_total}$ is the total conduction loss of DAB circuit, I_{DSon_RMS} is the MOSFET's drain current and R_{DSon} is the MOSFET's drain-source on-state resistance.

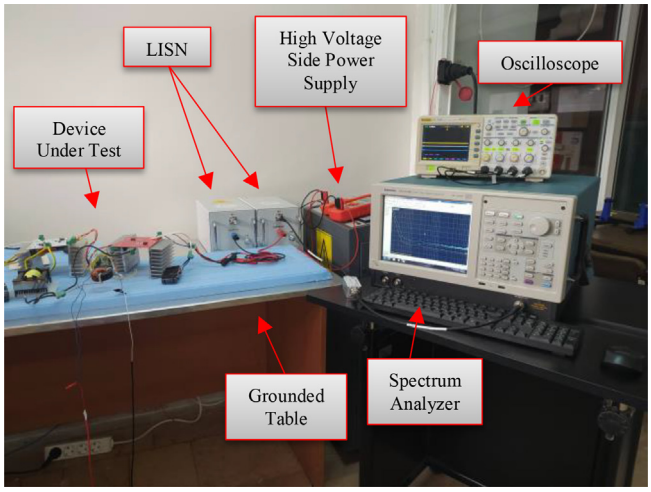

Fig. 6. ISUBÜ EMI Conducted Emission Laboratory.

The circuits will be named as Type1 (Si-based DAB circuit working with the SPS modulation), Type2 (Si-based DAB circuit working with the DPS modulation), Type3 (SiC-based DAB circuit working with the SPS modulation) and Type4 (SiC-based DAB circuit work-

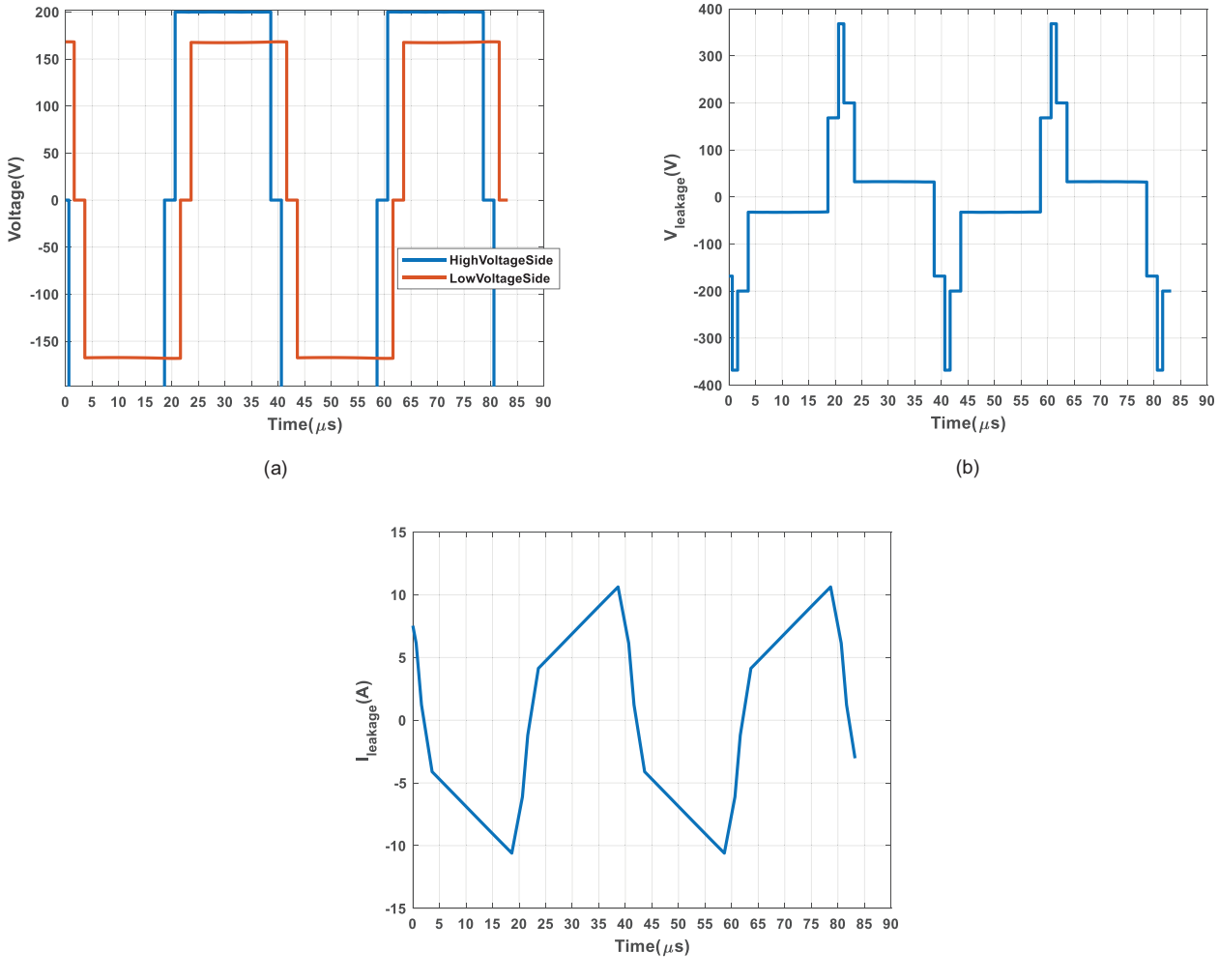

Fig. 5. Current on Leakage Inductance of Si Based DAB Circuit Working with DPS Modulation Method.

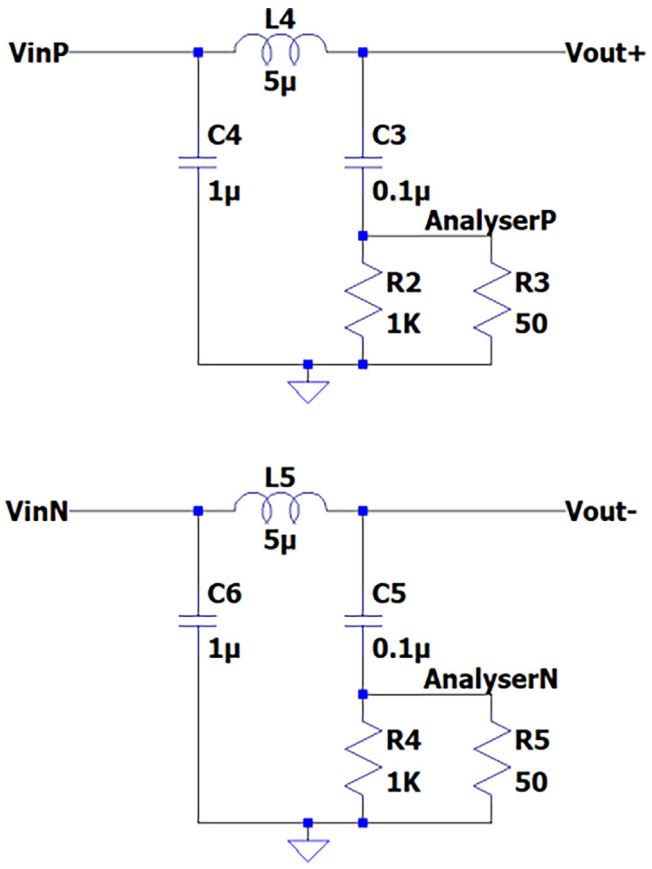

Fig. 7. Line Impedance Stabilization Network.

ing with the DPS modulation) in experimental results sections. Also all of MOSFETs are driven Infenion IR2103 half bridge MOSFET drivers. Since one driver is used for each half bridge, totally 4 drivers are used for every circuit.

3.1. Experimental results of circuit Type1

The current on the leakage inductance of circuit Type1 is simulated in Plecs and given in the Fig. 4. The RMS value of the current was calculated as 6.73A.

Using Equation (9), the conduction loss is calculated as 110 W. In the experimental environment, it has been observed that the input power was 1110 W while the output power was 980 W, and thus the circuit works with 130 W lost power and 88.5% efficiency.

3.2. Experimental results of circuit Type2

The current on the leakage inductance of the circuit Type2 is simulated in Plecs and given in the Fig. 5 and the RMS value of the current was calculated as 6.97A.

When the current waveform and RMS values are compared for circuit Type1 and Type2, it is seen that the average value of the current on the leakage inductance is higher in circuit Type2. In addition, since the current waveform is sawtooth rather than square wave, its peak value has reached 11A at circuit Type2. These will cause more stress on the switching elements because of EMI emitted by the parasitic components. As a result, for circuit Type2, it is expected that EMI is to be higher.

Using Equation (9), the conduction loss of circuit Type2 is calculated as 117 W. In the experimental observation, the input power was measured as 1060 W at the point where the output power was 941 W. It has been observed that the circuit works with 88% efficiency with 120 W lost power.

3.3. Experimental results of circuit Type3

The current ripple on the leakage inductance of the circuit Type3 is the same as the current ripple of the circuit Type1. The conduction loss of the circuit Type3 is calculated as 50 W using Equation (9) due to the low R_{DSon} resistance of SiC MOSFETs. However, in the experimental observation, it has been observed that the input power is 1180 W while output power is 1040 W. Thus, a loss of 140 W has been detected and it has been observed that the circuit operates with 88% efficiency.

3.4. Experimental results of circuit Type4

The current ripple on the leakage inductance of the circuit Type4 is the same as the current ripple of the circuit Type2. However, while the conduction loss was calculated as 47 W in this circuit, it has been observed that the input power is 1240 W while output power is 1010 W, and it was observed that the circuit oper-

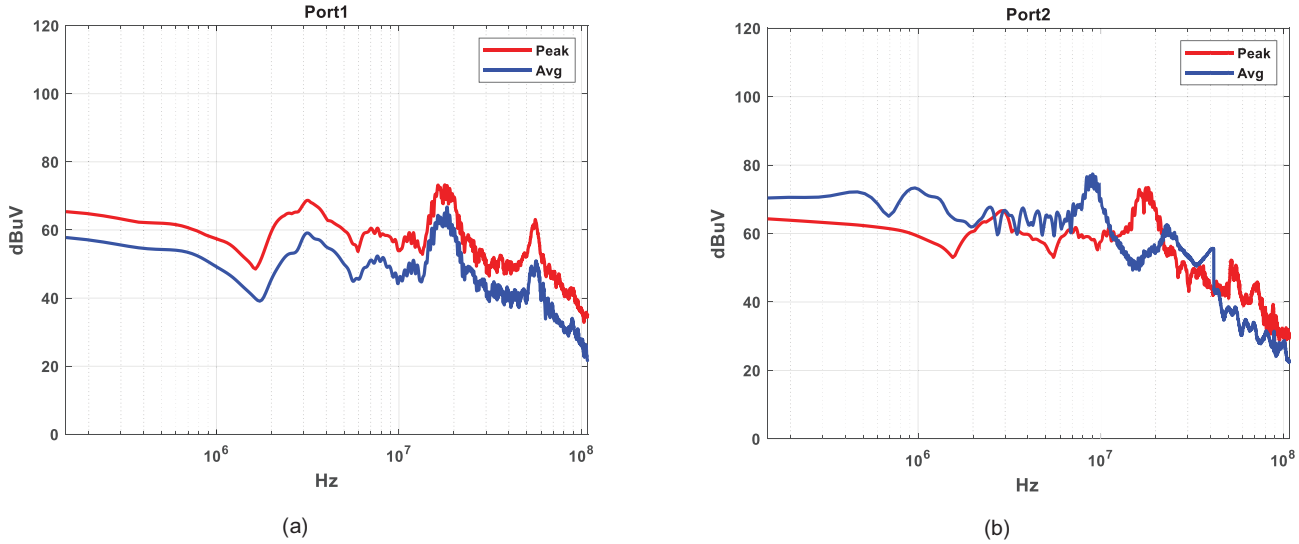

Fig. 8. DAB Circuit Peak and Average EMI measurement from (a) Port1 and (b) Port2.

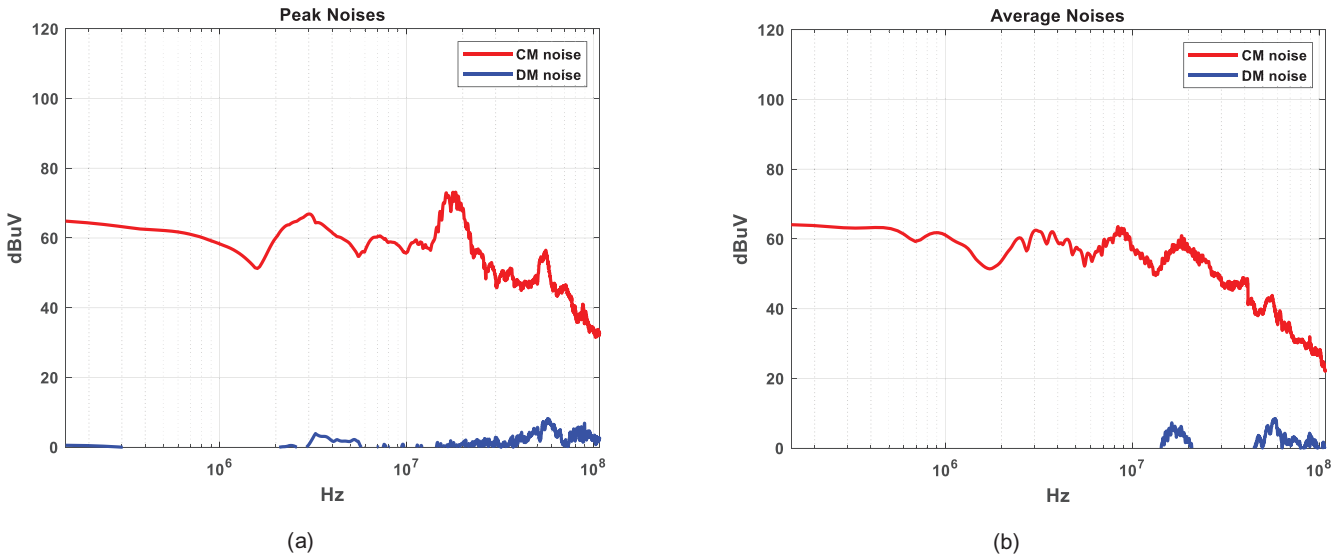

Fig. 9. DAB Circuit CM and DM conducted emissions for (a) Peak, (b) Average Noise.

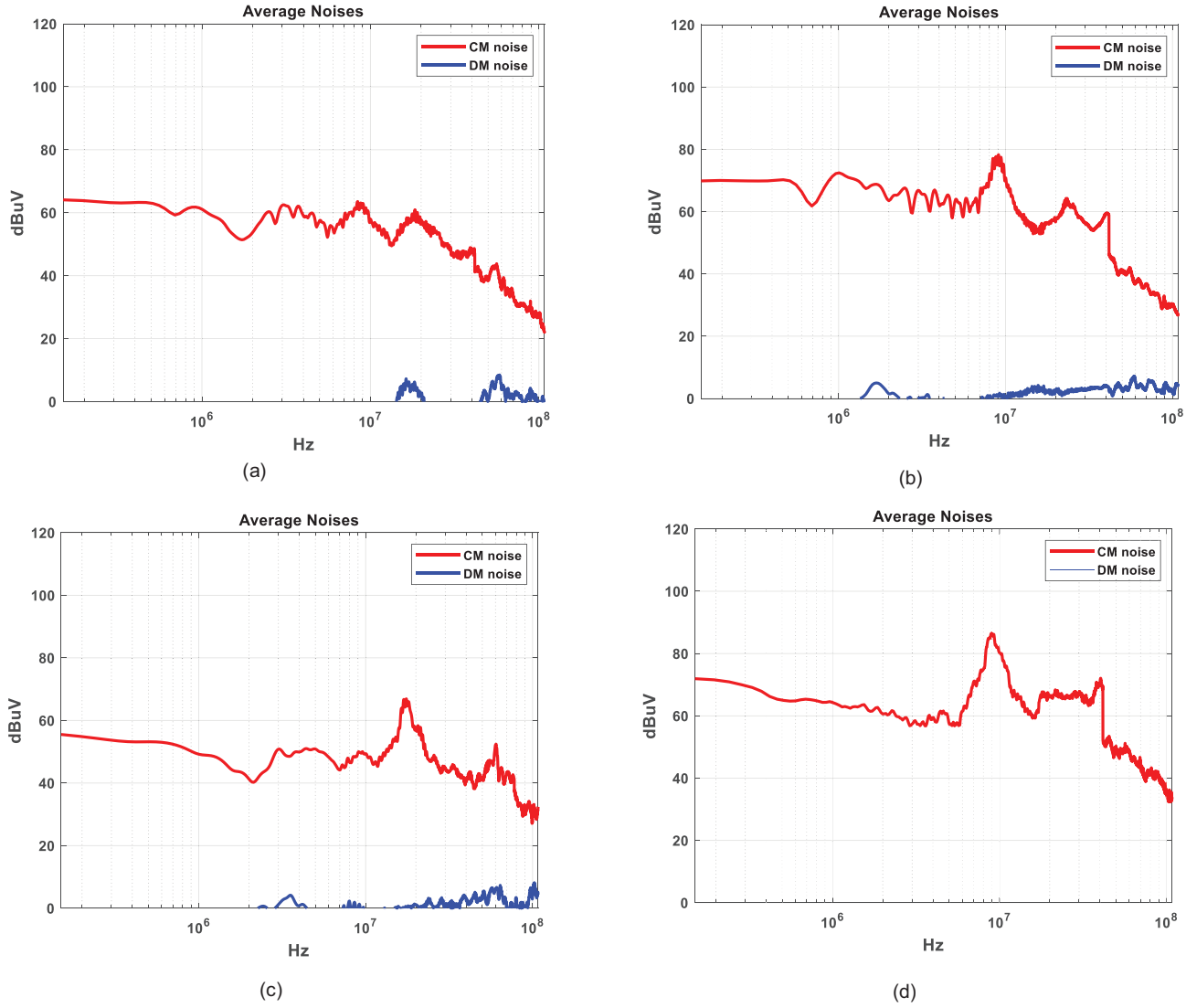

Fig. 10. The Average Noise of (a) Type1, (b) Type2, (c) Type3 and (d) Type 4 DAB Circuits.

ated with 82% efficiency with a lost power of 230 W. It is thought that circuit Type4 works with hard switching and high number of switching increased the switching losses.

4. Conducted emission results

EMI analyzes of the designed DAB circuits were performed in the EMI laboratory of Isparta University of Applied Sciences, which is shown in Fig. 6. Since our circuits are intended to be used in electric vehicles, in order to comply with the CISRP 25 standard [4], which deals with the electronic systems of electric vehicles and internal combustion vehicles, Line Impedance Stabilization Network (LISN) which is shown in Fig. 7 with an inductance value of 5uH was used in our experiments and the measurements were carried out in the frequency range of 150 kHz to 108 MHz.

In the first step, peak and average measurements of the circuit input as port1 and port2 were taken. In order to analyze the obtained measurements correctly, it is necessary to separate the EMI into CM and DM noise components. In the literature, the calculation of CM and DM noise components is given as shown in Equations (11) and (12) [22,31,26,28,25]. Accordingly, EMI measurement was made for circuit Type1 and the results given in Fig. 8 were obtained. By applying Equations (11) and (12) to the results obtained, the CM and DM noise components were obtained as given in Fig. 8.

$$v_{cm} = \frac{v_{port1} - v_{port2}}{2} \tag{11}$$

$$v_{dm} = \frac{v_{port1} + v_{port2}}{2} \tag{12}$$

here v_{port1} is the noise received from port1 input, v_{port2} is the noise received from port2 input, v_{cm} is the common mode noise and v_{dm} is the differential mode noise.

As we can see from Fig. 9, EMI in DAB circuits, as in other power electronics circuits, originates from the CM component. The DM noise component is negligible.

The CM noise made by Type1, Type2, Type3 and Type4 circuits in the experiments carried out is given in Fig. 10, respectively. It was observed that the peak values of the generated noise were 73, 88, 77 and 96dBuV respectively as given in Table 2.

EMI emission of Type1 and Type2 circuits working with SPS and DPS modulation method of Si Based DAB circuit is shown in Fig. 11-a. Looking at this figure, it is seen that the leakage inductance current of the Type2 circuit is higher than the average and peak value of the Type1 circuit. It is seen that the noise made by the Type2 circuit throughout the spectrum is much higher. The same result can be seen for the SiC-based DAB circuit by looking at Fig. 11-b. From here, we can understand that although the efficiency in the relevant circuits is almost the same, the current and voltage waveforms in the DPS modulation method can seriously change the EMI created by the circuit.

In addition, looking at the comparison in Fig. 12, it can be observed that SiC MOSFETs emit with much less conducted noise at the same efficiency. It has been observed that SiC MOSFETs emit EMI almost as much as Si MOSFETs, even when the switching loss is higher when compared to Type2 and Type4. It can be seen from here that by making soft switching instead of hard switching in SiC-based DAB circuits, besides increasing the efficiency, the conduction EMI can be seriously reduced.

Table 2
Experimental Results of DAB Circuits.

Type of Circuit	Type of Switching Element	Name of Switching Element	Phase Shift Method	EMI (dBμV)	Efficiency (%)
Type1	Si MOSFET	IRFP460s	SPS	73	88.5
Type2			DPS	88	88
Type3	SiC MOSFET	C2M0160120D	SPS	77	88
Type4			DPS	96	82

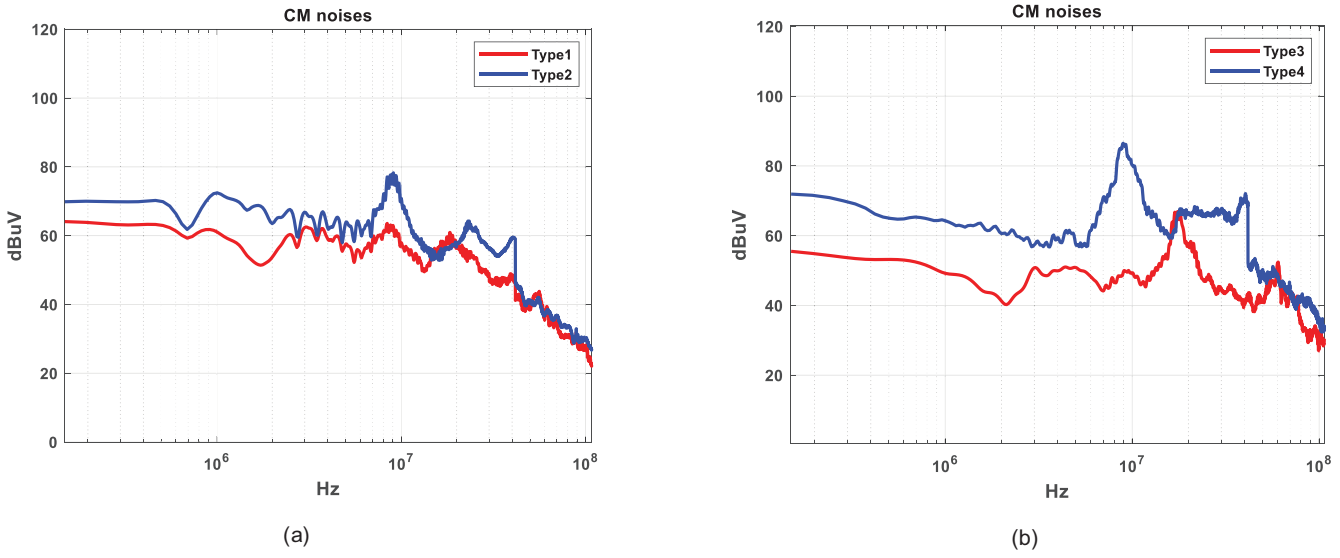

Fig. 11. EMI Comparison of (a) Type1 vs. Type2 and (b) Type3 vs. Type4.

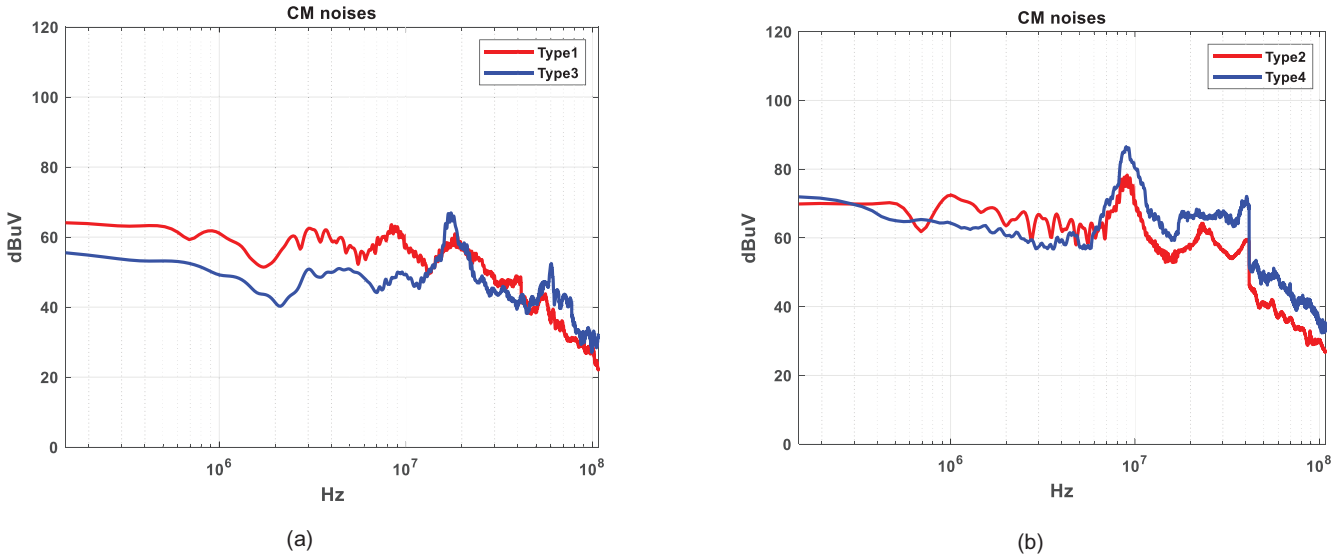

Fig. 12. EMI Comparison of (a) Type1 vs. Type3 and (b) Type2 vs. Type4.

5. Conclusion

In this study, the effects of modulation techniques and switching element type on conducted EMI were investigated using four different types of DAB circuits designed. In the literature, the studies are generally focused on DAB hardware design and filtering for EMI but the subject of this paper is not studied.

As a result of the experiments carried out, it has been observed that EMI caused by SPS modulation is 15–20 dBμV less than the EMI caused by DPS. This difference may be caused by the much more variation of the voltage waveform on the leakage inductance at DPS method. Moreover, it has been observed that SiC based DAB converter emits more EMI than Si based DAB converter. Efficiency values will vary according to the type of transistor used. It has been observed that the efficiencies of SiC based and Si based DAB converters working with SPS modulation are almost same. But when SiC based DAB circuit is operated with DPS, its efficiency is lower than SPS modulation. If study is carried on the relationship between SPS, DPS and EMI, the accuracy of this study will be understood. In future studies, improvements in modulation techniques will reduce EMI and the effect of this situation on efficiency will be examined. Also the effects of EPS and TPS modulations' mods on conducted EMI will be analyzed and present to the literature.

Declaration of Competing Interest

The authors declare that they have no known competing financial interests or personal relationships that could have appeared to influence the work reported in this paper.

Acknowledgments

This study was supported by Isparta University of Applied Sciences Scientific Research Projects Coordination Unit (BAP) with BTAP 2020-BTAP2-0091.

References

[1] N. Arı, Ş. Özen, Elektromanyetik Uyumluluk, Palme Yayıncılık, Ankara, 2000.
[2] H. Bai, C. Mi, Eliminate reactive power and increase system efficiency of isolated bidirectional dual-active-bridge DC–DC converters using novel dual-phase-shift control, IEEE Trans. Power Electron. 23 (6) (2008) 2905–2914.
[3] Y. Chu, S. Wang, A generalized common-mode current cancelation approach for power converters. 62(7).
[4] CISPR25. Vehicles, boats and internal combustion engines – Radio disturbance characteristics – Limits and methods of measurement for the protection of on-board receivers, 2008.
[5] H. Dogan, I.B. Basyigit, A. Genc. Variation of Radiated Emission from Heatsinks on PCB according to Fin Types. 2019 3rd International Symposium on Multidisciplinary Studies and Innovative Technologies (ISMSIT), 2019. Ankara, Turkey: IEEE.
[6] B. Dwiza, J. Kalaiselvi, Analytical approach for common mode EMI noise analysis in dual active bridge converter, in: IECON 2020 the 46th Annual Conference of the IEEE Industrial Electronics Society, IEEE, Singapore, 2020, pp. 1279–1284.
[7] X. Fei, Z. Feng, N. PuQi, W. Xuhui. Analyzing ZVS Soft Switching Using Single Phase Shift Control Strategy of Dual Active Bridge Isolated DC-DC Converters. 2018 21st International Conference on Electrical Machines and Systems (ICEMS), 2018, 2378–2381.
[8] A. Genç, H. Doğan, İ.B. Başyiğit, S. Helhel, Heatsink Preselection chart to minimize radiated emission in broadband on the PCB, IEEE Trans. Electromagn. Compat. (2020) 419–426.
[9] H. Geramirad, F. Morel, P. Dworakowski, P. Camail, B. Lefebvre, T. Lagier, C. Vollaire, Experimental EMI study of a 3-phase 100kW 1200V dual active bridge converter using SiC MOSFETs, 2020 22nd European Conference on Power Electronics and Applications (EPE'20 ECCE Europe), IEEE, Lyon, France, 2020.
[10] S.A. Gorji, H.G. Sahebi, M. Ektesabi, A.B. Rad, Topologies and control schemes of bidirectional DC–DC power converters: an overview, IEEE Access 7 (2019) 117997–118019.
[11] Y.A. Harrye, K. Ahmed, G. Adam, A. Aboushady, Comprehensive steady state analysis of bidirectional dual active bridge DC, DC converter using triple phase shift control, in: IEEE 23rd International Symposium on Industrial Electronics (ISIE), IEEE, Istanbul, Turkey, 2014, pp. 437–442.
[12] M.J. Heller, F. Krismer, J.W. Kolar, EMI filter design for the integrated dual three-phase active bridge (D3AB) PFC rectifier, IEEE Trans. Power Electron. 37 (12) (2022) 14527–14546.
[13] J. Huang, Y. Wang, Z. Li, W. Lei, Unified triple-phase-shift control to minimize current stress and achieve full soft-switching of isolated bidirectional DC–DC converter, IEEE Trans. Ind. Electron. 63 (7) (2016) 4169–4179.
[14] J. Kang, X. Zhu, L. Yun. Application of Random PWM Technology in DAB Converter. 2018 IEEE International Power Electronics and Application Conference and Exposition (PEAC), 2018 (pp. 1-6). Shenzhen, China: IEEE.
[15] G. Kapino, W.-T. Franke, 2019. Loss Comparison for Different Technologies of Semiconductors for Electrical Drive Motor Application. 13th International Conference on Compatibility, Power Electronics and Power Engineering (pp. 1–5). Sonderborg, Denmark: IEEE.
[16] A. Kızıcı, Design and Implementation of A Hıgh Power Density Dual Active Bridge DC/DC Converter With GaN Power Transistors, Hacettepe University, Ankara, Turkey, 2019.
[17] F. Krismer, Modeling and Optimization of Bidirectional Dual Active Bridge DC-DC Converter Topologies, ETH Zurich, 2010. Ph.D. dissertation.
[18] A. Kumar, A.H. Bhat, P. Agarwal. Comparative analysis of dual active bridge isolated DC to DC converter with single phase shift and extended phase shift control techniques. 2017 6th International Conference on Computer Applications In Electrical Engineering-Recent Advances (CERA), 2017. Roorkee, India.

[19] B.M. Kumar, A. Kumar, A.H. Bhat, P. Agarwal. Comparative study of dual active bridge isolated DC to DC converter with single phase shift and dual phase shift control techniques. 2017 Recent Developments in Control, Automation Power Engineering (RDCAPE). Noida, India, 2017.
[20] S. Kumar, S.K. Voruganti, G. Gohil. Common-mode Current Analysis and Cancellation Technique for Dual Active Bridge Converter based DC System. 2019 IEEE Energy Conversion Congress and Exposition (ECCE). Baltimore, MD, USA: IEEE, 2019.
[21] S. Kumar, S.K. Voruganti, B. Akin, G. Gohil, Common-mode current analysis and cancellation technique for dual active bridge converter based DC system, IEEE Trans. Ind. Appl. 58 (4) (2022) 4955–4966.
[22] F.W. Ling Jiang, 2021. A Practical Method for Separating Common-Mode and Differential-Mode Emissions in Conducted Emissions Testing. Analog Dialogue.
[23] S. Maniktala, Switching Power Supplies A–Z, Elsevier, Oxford, 2012.
[24] G.G. Oggier, G.O. GarcÍa, A.R. Oliva, Switching control strategy to minimize dual active bridge converter losses, IEEE Trans. Power Electron. 24 (7) (2009) 1826–1838.
[25] R. Ozenbaugh, Emi Filter Design, second ed., Markel Dekker Inc., New York, 2001.
[26] C.R. Paul, Introduction to Electromagnetic Compatibility, Second ed., A John Wiley & Sons, Inc. Publication, New Jersey, 2006.
[27] D. Ravi, B. Mallikarjuna Reddy, P. Samuel, Bidirectional dc to dc converters: an overview of various topologies, switching schemes and control techniques, Int. J. Eng. Technol. 7 (4.5) (2018) 360.
[28] S.L. Richard Anslow, How to Get the Best Results Using LTspice for EMC Simulation—Part 1, Analog Devices, 2021.
[29] G.-J. Su. Comparison of Si, SiC, and GaN based Isolation Converters for Onboard Charger Applications. 2018 IEEE Energy Conversion Congress and Exposition (ECCE). Portland, OR, USA: IEEE, 2018.
[30] Texas Instruments. Bi-Directional, Dual Active Bridge Reference Design for Level 3 Electric Vehicle Charging Stations. ti.com, 2019.
[31] S. Wang, F. Lee, W. Odendaal, Characterization, evaluation, and design of noise Separator for conducted EMI noise diagnosis, Power Electr., IEEE Trans. 20 (4) (2005) 974–982.
[32] I. Wolfspeed. Discrete Silicon Carbide MOSFETs. Retrieved from Wolfspeed: https://www.wolfspeed.com/products/power/sic-mosfets, 2022.
[33] Y. Yuchen, EMI Noise Reduction Techniques for High Frequency, Diss. Virginia Tech, Virginia, 2018.
[34] S. Zengin, Single-Stage Dual Active Bridge AC-DC Converter using Silicon Carbide (SIC) Power Switches, Ege University, İzmir, Turkey, 2019.
[35] B. Zhao, Q. Song, W. Liu, Power characterization of isolated bidirectional dual-active-bridge DC–DC converter with dual-phase-shift control, IEEE Trans. Power Electron. 27 (9) (2012) 4172–4176.
[36] R. Zhong, Y. Chen, Z. Chen, C. Bi, A. Zhou, Common-mode conducted EMI prediction for dual active bridge converter based on unterminated behavioral model, IEEE J. Emerg. Selected Topics Power Electr. 10 (6) (2022) 7205–7213.